LBL-24906
Preprint

Lawrence Berkeley Laboratory
UNIVERSITY OF CALIFORNIA

Materials & Chemical Sciences Division

Submitted to Journal of the
Electrochemical Society

Electrode Kinetics of Organodisulfide Cathodes for Storage Batteries

M. Liu, S.J. Visco, and L.C. De Jonghe

March 1989

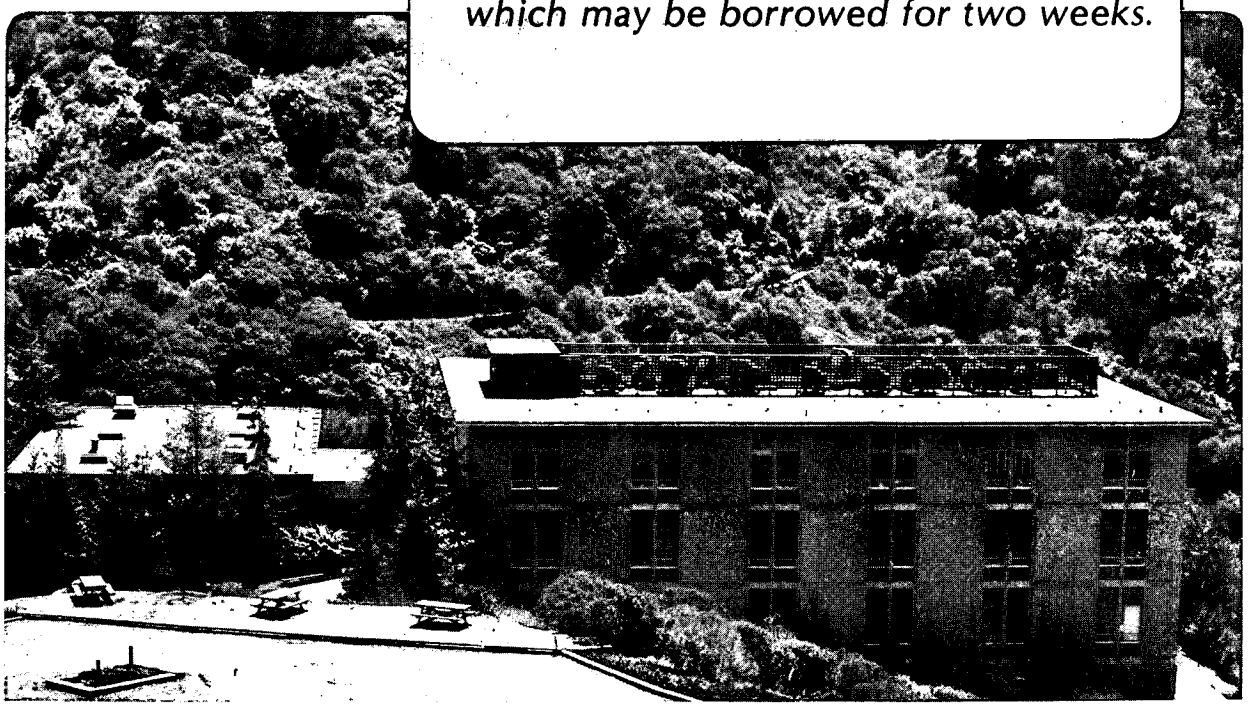

Prepared for the U.S. Department of Energy under Contract Number DE-AC03-76SF00098.

DISCLAIMER

LBL # 24906

ELECTRODE KINETICS OF ORGANODISULFIDE CATHODES FOR STORAGE BATTERIES

Meilin Liu, Steven J. Visco, and Lutgard C. De Jonghe

Department of Materials Science and Mineral Engineering
University of California
and
Materials and Chemical Sciences Division
Lawrence Berkeley Laboratory
1 Cyclotron Road
Berkeley, CA 94720

This work was supported by the Assistant Secretary for Conservation and Renewable Energy, Office of Energy Storage and Distribution, Energy Storage Division of the U.S. Department of Energy under Contract No. DE-AC03-76SF00098.

ABSTRACT

The electrode kinetics of a diverse group of organodisulfide cathode materials have been systematically investigated. The electrochemical behavior of these redox couples was studied as a function of the organic moiety (R) in the organodisulfide species (RSSR). These studies were performed with a variety of working electrodes, including platinum, glassy carbon, graphite, stainless steel, aluminum, and copper. The possible reaction pathways and mechanisms have been intuitively proposed, theoretically analyzed, and experimentally verified. Observations showed that while electron transfer-rate constants varied with organic moiety, the mechanistic details of the redox path were invarant with the R groups of the organodisulfide compounds (RSSR). The reaction mechanism, as determined from experimental observations, can be expressed as

(1) $2\ [\ RS^{-} \rightarrow RS\bullet + e^{-}\ ]$

(2) $RS\bullet + RS\bullet = RSSR$

for the oxidation of thiolate anions (RS^{-}) to the corresponding organodisulfides. The first step in the redox mechanism, charge transfer, is rate determining, while the second step, chemical reaction, is at equilibrium. The observed transfer coefficients are quite asymmetric and vary as a function of the R group in RSSR and the electrode materials. The standard rate constants are also affected by the nature of the organic moiety, R, and are in the range of 10^{-8} to 10^{-6} from ambient to 100°C. Further, and in purticular, enhanced electron transfer rates have been achieved by the addition of several electrocatalysts.

Introduction

Advanced high temperature secondary batteries incorporating solid electrolyte separators offer many advantages over conventional cells, including high specific energy and power density, as well as excellent charge retention on storage due to negligible self discharge. Still, the impressive performance of these cells is offset somewhat by the technical difficulties of operating batteries at high temperatures. Accordingly, various efforts have been made to introduce alternative high specific power/energy batteries operating at reduced temperatures[1-4], including the sodium/β"-alumina/RSSR cell[5]. However, since mass transport and electrode kinetics are thermally activated, a thorough understanding of these processes is necessary for successful operation of lower temperature systems.

It is well known that the efficiency and power of an electrochemical energy conversion system increases with increasing electrode kinetics and mass transport, and with decreasing internal resistance. Accordingly, for batteries such as the alkali metal/organodisulfide cells[5], the critical limitations on charge transfer rates are essentially determined by the nature of the positive electrode. Although the electrode reactions of organodisulfide/thiolate redox couples have been reported previously to be kinetically hindered[6,7], particularly at ambient temperatures, their reversibility can be substantially enhanced by introducing appropriate electrocatalysts. The identification of effective catalysts, however, can only emerge from a detailed understanding of the kinetic mechanisms that control the overall process.

The investigation of electron-transfer reaction kinetics generally

involves the determination of *reaction route, mechanism*, and *kinetic parameters*[8]. The *reaction route* refers to a successive sequence of elementary reactions which constitute the overall, stoichiometric electrode reaction. The *mechanism* specifies the rate-controlling nature of the constituent steps and their coupling[9]. The basic *kinetic parameters* characterizing an electrode reaction include: (1) the reaction order, (2) the standard rate constant or exchange current density, (3) the symmetry factor for the rate determining step (rds) or apparent transfer coefficients, (4) the stoichiometric coefficients, and (5) the activation energy. The above parameters can be determined from the dependence of reaction rate (i.e., current) on various observables, including overpotential across the interface, composition of the electrolytic solution adjacent to the electrode, the nature of the electrode surface, and temperature.

The purpose of this study is to elucidate the kinetic behavior of a diverse group of organodisulfide/thiolate redox couples, and to provide a basis for identifying effective electrocatalysts for activation of these redox reactions. The effect of temperature on electrode kinetics as well as on transport properties will be addressed in a subsequent communication[10].

Experimental

Organosulfur compounds [tetramethylthiuram disulfide (TMTD), tetraethylthiuram disulfide (TETD), phenyl disulfide (PDS), di-fluorophenyl disulfide (FPDS), sodium diethyl dithiocarbamate (NaDEDC), sodium dimethyl dithiocarbamate (NaDMDC)], supporting electrolyte [tetraethylammonium perchlorate (TEAP)], reference electrode filling electrolyte

[tetramethylammonium chloride (TMAC)], and dimethylsulfoxide (DMSO) were prepared and stored as described in a previous publication[6]. Dimethyldisulfide (DMDS) was obtained from Aldrich* and distilled under vacuum over molecular sieves. Transition metal phthalocyanines (MPc), were obtained from Pfaltz & Bauer** and stored in an argon atmosphere dry box.

An Ag/AgCl reference electrode† was connected to the working electrode compartment with a Luggin capillary salt bridge containing a 0.1 M TEAP solution. The reference electrode compartment contained a 0.1 M TMAC aqueous solution saturated with AgCl.

Three-electrode electroanalytical cells with platinum auxiliary electrodes were used throughout the experiments. Planar disks (diameter = 0.8 cm) of platinum, glassy carbon, graphite, stainless steel, aluminum, and copper metal were used as the working electrodes. Before each experiment, the working electrodes were polished to a mirror finish with diamond paste (1μm) and rinsed with acetone. Unless otherwise stated, the electrolyte solution consisted of 0.1 M TEAP in DMSO. The electrolyte solutions were purged with dry argon for about 10 minutes prior to experimentation and continuously purged at a slower rate during each measurement.

In *rotating disk voltammetry*[11-13], linear or triangular potential functions, generated by a PAR 173 Potentiostat/Galvanostat†† in conjunction with a PAR 175 Universal Programmer††, were applied to a disk electrode immersed in the electrolyte solution (150 cm^3). The rotation speed of the disk electrode was modulated with an ASR Electrode Rotator††† and Speed Controller†††. The

---

* Aldrich Chemical Company, Inc., 940 West Saint Paul Avenue, Milwaukee, Wisconsin 53233.

** Pfaltz & Bauer, Inc., 172 E. Aurora St., Waterbury, Ct. 06708.

† Astra Scientific.

†† Princeton Applied Research, 26102 Eden Landing Road, Suite 3, Hayward, California 94545

††† Pine instrument Co., 101 Industrial Drive, Grove City, PA 16127.

corresponding current response was either recorded with a 4120T Bascom-Turner digital recorder[‡] or acquired with an IBM-PC/AT computer through a DT2801A data translation board[‡‡] using ASYSTANT[‡‡‡] software. The potential sweep rates ranged from 1 mV/s to 10 mV/s. Solution viscosities were measured using an Ostwald viscometer.

In *linear* and *Tafel polarization measurements*, the potential was stepped by a PAR 173 potentiostat/Galvanostat[††] and the corresponding currents at each potential were recorded using a Bascom-Turner recorder[‡]. Complications due to mass transfer were eliminated by either stirring the electrolyte solution with a magnetic bar when a stationary electrode was used, or by measuring the current at a RDE at high rotation speed (about 3000 rpm).

Sodium/β"-alumina/RSSR cells were galvanostatically controlled by an IBM-PC/AT computer through a DT2801A data translation board[‡‡] and a PAR 173 potentiostat/Galvanostat[††] using ASYST[‡‡‡] software, while the corresponding cell voltages were simultaneously acquired by the computer.

Kinetic equations[14-18]

It was determined previously that the overall, stoichiometric reaction for organodisulfide/thiolate redox couples can be described as[6]

$$RSSR + 2\,e^- = 2\,RS^- \qquad [1]$$

Under the assumption that complications due to electrode adsorption are

‡ Bascom-Turner, Inc., 111 Downey Street, Norwood, MA 02062

‡‡ Data Translation, Inc., 100 Locke Drive, Marlborough, Massachusetts 01752-1192

‡‡‡ Macmillan Software Company.

negligible, the relationship between current, i, and overpotential at the electrode surface, η, can be described by[14,16]

$$i = i_o\{(C_{RS^-,s}/C_{RS^-,b})^{\gamma_{RS^-}} \exp(\alpha_a F\eta/RT) - (C_{RSSR,s}/C_{RSSR,b})^{\gamma_{RSSR}} \exp(-\alpha_c F\eta/RT)\} \quad [2]$$

where i_o is the exchange current, γ_{RS^-} and γ_{RSSR} are the anodic and cathodic reaction orders for species RS^- and RSSR, and $C_{i,s}$ and $C_{i,b}$ are the concentrations of species i at the electrode surface and in the bulk solution, respectively. The anodic and cathodic transfer coefficients, α_a and α_c, can be expressed as[16]

$$\alpha_a = \vec{\gamma}/\nu + r\,(1 - \beta) \quad [3a]$$

$$\alpha_c = \overleftarrow{\gamma}/\nu + r\,\beta \quad [3b]$$

where $\vec{\gamma}$ is the number of electrons transferred in the steps *preceding* the rds, $\overleftarrow{\gamma}$ is the number of electrons transferred in the steps *after* the rds, r is the number of electrons transferred in the rds, ν is the stoichiometric coefficient, and β is the symmetry factor of the rds.

The exchange current can, in general, be expressed as[15]

$$i_o = (n/\nu)FA\,k^o\,(C_{RS^-})^{\mu}\,(C_{RSSR})^{\lambda} \quad [4]$$

where n is the total number of electrons involved in the overall reaction, k^o is the standard rate constant, and the exponents μ and λ are constant dependent on the reaction mechanism.

Under the condition that the electrode reaction is completely controlled by kinetics, i.e. mass transfer is sufficiently fast to ensure that the concentration of the electroactive species at the electrode surface is identical to the bulk concentration, Eqn.2 can be reduced to the Butler-Volmer

equation

$$i_k = i_o \{ \exp(\alpha_a F\eta/RT) - \exp(-\alpha_c F\eta/RT) \} \quad [5]$$

Mechanistic analysis[15,16]

Listed in Table I are a number of possible reaction pathways considered in the analysis, EC, ECE, CEE, and EEC route, together with the corresponding reaction mechanisms. The kinetic parameters associated with each mechanism, such as reaction orders, transfer coefficients, and dependence of exchange current densities on concentration, can be derived as follows.

First, assume the reaction takes the EC route (see Table I). Then, the reaction rate for each elementary step can be expressed as[15]

$$r_1 = i_1/F = k_{a1} C_{RS^-} \exp[(1-\beta_1)FE/RT] - k_{c1} C_{RS^\bullet} \exp[-\beta_1 FE/RT] \quad [6a]$$

$$r_2 = k_f (C_{RS^\bullet})^2 - k_b C_{RSSR} \quad [6b]$$

Depending on the rate-controlling nature of each step, two possible reaction mechanisms result.

(1) The first step, charge transfer, is the rate-determining step (rds) and the second step, chemical reaction, is at equilibrium. In this case, the concentration of the radical RS• is given by

$$C_{RS^\bullet} = (k_b/k_f C_{RSSR})^{1/2} \quad [7]$$

and the overall reaction rate can be expressed as

$$r_1 = i_1/F = k_{a1} C_{RS^-} \exp[\alpha_a FE/RT] - k_{c1} (k_b/k_f C_{RSSR})^{1/2} \exp[-\alpha_c FE/RT] \quad [8a]$$

or

$$i = i_o\{(C_{RS^-,s}/C_{RS^-,b})\exp(\alpha_a F\eta/RT) - (C_{RSSR,s}/C_{RSSR,b})^{1/2}\exp(-\alpha_c F\eta/RT)\} \quad [8b]$$

where

$$i_o = FAk^o\ (C_{RS^-})^{\alpha_c}\ (C_{RSSR})^{\alpha_a/2}, \quad [9]$$

indicating that $\mu = \alpha_c$ and $\lambda = \alpha_a/2$. The standard rate constant can be expressed by the rate constants associated with each elementary step as

$$k^o = (k_{a1})^{\alpha_c}(k_{c1})^{\alpha_a}(k_b/k_f)^{\alpha_a/2}. \quad [10]$$

In this case, the reaction order for species RS^- and RSSR are 1 and 1/2, respectively. The transfer coefficients are related to the symmetry factor as

$$\alpha_c = \beta_1 \quad [11a]$$

$$\alpha_a = 1 - \beta_1. \quad [11b]$$

(2) If the chemical reaction is the rds and the charge-transfer step is at equilibrium, then the overall reaction rate can be expressed as

$$i = i_o\ \{\ (C_{RS^-,s}/C_{RS^-,b})^2\ \exp(2F\eta/RT) - (C_{RSSR,s}/C_{RSSR,b})\ \} \quad [12]$$

where

$$i_o = 2\ FA\ k^o\ C_{RSSR} \quad [13]$$

and

$$k^o = k_b. \quad [14]$$

In this case, the reaction order for species RS^- is 2 and that for species RSSR is 1. The corresponding anodic and cathodic transfer coefficients are 2

and 0, respectively, indicating that the reaction rate in the cathodic direction is independent of electrode potential. Further, the exponents for the concentration dependence of exchange currents are 1 for λ and 0 for μ, indicating that i_o is independent of the concentration of thiolate anions.

Similar analyses have been performed for other possible reaction pathways, i.e., the *ECE*, *CEE*, and *EEC* route in Table I.

The governing kinetic equations and the corresponding reaction orders, transfer coefficients, and stoichiometric coefficients for the nine possible reaction mechanisms derived from the above four possible reaction pathways have been tabulated in Table II. The corresponding expression for the exchange current and its dependence on concentration, as defined in Eqn.4, were summarized in Table III for the various reaction mechanisms.

Electrochemical Methods

Rotating Disk Electrode Techniques[19-21]

Reaction orders for various organodisulfides and the corresponding thiolate anions were determined from the dependence of the current at an RDE with rotation speed at constant electrode potential without varying the bulk concentration (since the effective concentration of electroactive species at the surface of an RDE is a function of rotation speed).

The current at an RDE can, in general, be expressed as

$$i = i_l \left[1 - c_{i,s}/c_{i,b} \right] \qquad [15a]$$

where i_l is the convective-diffusive limiting current given by

$$i_l = 0.62\ (nFA)C^{*}_{i,b}D_i^{2/3}\nu^{-1/6}\omega^{1/2} \qquad [15b]$$

Combining Eqn.2 and 15, one can relate the anodic or cathodic current at an RDE, i, to i_l and i_k as

$$i/i_k = [\ 1 - i/i_l\ ]^{\gamma_i} \qquad [16]$$

where i_k is the *pure* kinetic current (as defined in Eqn.5). At a given potential, the kinetic current is a constant (and can be determined from extrapolation at $\omega \to \infty$). The reaction order for species i, γ_i, can be expressed as

$$\gamma_{RS-} = d[\log(i_a)]/d[\log(1 - i_a/i_{l,a})] \qquad [17a]$$

and

$$\gamma_{RSRS} = d[\log(i_c)]/d[\log(1 - i_c/i_{l,c})] \qquad [17b]$$

where i_a (or i_c) is the current measured at a given rotation speed and $i_{l,a}$ (or $i_{l,c}$) is the convective-diffusive limiting current at the same rotating speed.

When $\gamma_i = 1$, i.e., the reaction is first order for species i, Eqn.16 can be rewriten as

$$1/i = 1/i_k + 1/i_l \qquad [18]$$

Thus, the plot of 1/i vs. $\omega^{-1/2}$ at a constant potential is a straight line. The intercepts ($1/i_k$) give an estimate of kinetic current (i_k) at a given potential, while the slopes ($d(i^{-1})/d(\omega^{-1/2})$) allow assessment of the diffusion coefficients.

Polarization Measurement

Exchange currents, transfer coefficients, and stoichiometric coefficients were determined from polarization measurements at either stationary electrodes or rotating disk electrodes under experimental constraints that the electrochemical processes were completely controlled by kinetics.

When $|\eta| >> RT/F$, the Tafel approximation of Eq.5 gives

$$i_a = i_o \exp(\alpha_a F\eta/RT) \qquad [19a]$$

and

$$i_c = i_o \exp(-\alpha_c F\eta/RT) \qquad [19b]$$

The exchange currents were obtained directly from the intercepts of the Tafel plots. The anodic and cathodic transfer coefficients were calculated from the Tafel slopes. The stoichiometric coefficients were determined from the transfer coefficients and the total number of electrons involved in the overall reaction as

$$\nu = n / (\alpha_a + \alpha_c) \qquad [20]$$

When $|\eta| << RT/F$, linear approximation of Eq.5 gives

$$i_k = i_o (\alpha_a + \alpha_c) (F\eta/RT) \qquad [21]$$

The slope of the linear plot of i_k against η allows determination of exchange current, i_o. The standard rate constants were calculate from i_o's using Eqn.4.

The dependence of the exchange current on concentration was further used to verify the transfer coefficients and the reaction mechanism. The

theoretical values of μ and λ corresponding to different reaction mechanisms are tabulated in Table III.

Results and discussion

Reaction order (mechanism determination)

Linear sweep voltammograms at a platinum disk electrode, rotated at different rates, are shown in Fig.1(a) for oxidation of the thiolate anion FPT^- to the disulfide FPDS. The convective-diffusive limiting currents in the anodic direction, $i_{l,a}$, are shown in Fig.1(b) for oxidation of various thiolate anions to the corresponding disulfides. The slight deviation from linearity, particularly at high rotation rates, was probably due to the distortion of the hydrodynamic layer near the disk electrode by turbulant flow. The measured solution viscosity and calculated diffusion coefficients of the thiolate anions in the electrolyte solution are tabulated in Table IV.

The plots of log i_a vs. $\log(1-i_a/i_{l,a})$ for oxidation of FPT^- to FPDS at constant potentials and different rotation speeds are shown in Fig.2(a). The slope of the plots at different potentials represents the observed anodic order, γ_{FPT^-}, for species FPT^-.

As analyzed in the previous section and shown in Table II, the anodic reaction order for species RS^- should be either 1 or 2 for the mechanisms considered. The observed reaction orders, averaged over values obtained at different potentials from plots similar to Fig.2(a), are listed in Table V for oxidation of various thiolate anions. The experimental values of γ_{RS^-} are reasonably close to unity indicating that the oxidation of RS^- to RSSR is a first order reaction. In addition, the *linear* relationship between i^{-1} and

$\omega^{-1/2}$ at constant potentials, as shown in Fig.3(a), further confirms that the anodic order for species RS^- is one. This observation strongly suggests that reaction mechanisms with anodic reaction order of 2 are very unlikely, and the only plausible mechanisms left are those with oxidation reaction orders of 1, i.e., mechanism 1, 3, and 8.

Similarly, shown in Fig.2(b) are the plots of log $|i_c|$ vs log$[1-i_c/i_{l,c}]$ at different potentials for reduction of TETD to $DEDC^-$. The slopes or cathodic reaction orders obtained from similar plots for various disulfides are tabulated in Table V. The observed values are very close to 0.5 indicating that the reduction of RSSR to RS^- is a half order reaction.

Accordingly, the determination of reaction orders, in this case, uniquely suggests that the electrode reaction takes the EC route with the first step, charge transfer, as rate-determining step, i.e.,

$$2\ [\ RS^- \rightarrow RS\bullet + e^-\ ] \qquad [22a]$$

$$RS\bullet + RS\bullet = RSSR \qquad [22b]$$

Transfer coefficient, rate constant, and stoichiometric coefficient

Shown in Fig.3(b) are the Tafel plots constructed from the kinetic currents ($i_{k,a}$) obtained at $\omega \rightarrow \infty$ for oxidation of RS^- to RSSR. The kinetic currents in the anodic direction, $i_{k,a}$, were determined from the intercepts with the i^{-1} axis in the reciprocal Levich plot (i.e., i^{-1} vs $\omega^{-1/2}$) as shown in Fig.3(a). The anodic transfer coefficients, calculated from the Tafel slopes are listed in Table V. Since the reduction of RSSR to RS^- is a half order reaction, the plot of i^{-1} vs $\omega^{-1/2}$ for reduction is not a straight line (Eqn.18 is not valid) and hence the kinetic current in the cathodic direction,

$i_{k,c}$, can not be extrapolated from a plot similar to those for the anodic kinetic current. Instead, the cathodic kinetic currents were approximated by the currents directly measured at an RDE while increasing the rotation speed up to 3000 rpm; at low overpotentials i_k is well below i_l, so that the approximation is adequate.

Shown in Fig.4(a) are the currents directly measured at a platinum RDE for various organodisulfide/thiolate redox couples. The deviation from linear Tafel behavior observed at high overpotentials was brought about by mass transfer limitations. At these potentials, electrode kinetics were sufficiently rapid so that mass transport of the electroactive species to and from the electrode surface was unable to maintain the surface concentration close to the bulk concentration. Still, there does exist a sufficiently wide potential range over which Tafel behavior prevails and the Tafel slopes are well defined. The transfer coefficients and stoichiometric coefficients calculated from these Tafel slopes within this range and the standard rate constants estimated from the intercepts are tabulated in Table VI for different RSSR/RS^- couples.

The experimentally determined transfer coefficients and stoichiometric coefficients further confirm that the electrode reaction is correctly described by Eqn.22 (mechanism 1).

Concentration dependence

Polarization measurements were also performed on electrolyte solutions having various concentrations of organodisulfides and their corresponding thiolate salts. Cell currents between a platinum-disk working electrode and

a platinum counter electrode were measured at rotation speed of 3000 rpm. The exchange currents were then determined from the intercepts of the corresponding Tafel plots and the slopes of the linear polarization plots.

Figure 5(a) shows the dependence of i_o on C_{RS^-} for various redox couples at a constant bulk concentration of organodisulfide. The slopes of the plots, $d\{\log(i_o)\}/d\{\log(C_{RS^-})\}$, directly yield the kinetic parameter μ. Figure 5(b) shows the dependence of i_o on C_{RSSR} at a constant concentration of the corresponding thiolate salt. The slopes of these plots, $d\{\log(i_o)\}/d\{\log(C_{RSSR})\}$, allows estimation of the kinetic parameter λ. Deviations from linearity indicates that the exponents, μ and λ , or the transfer coefficients vary slightly at different concentrations. Nevertheless, the average values, as listed in Table VII, agree reasonably well with the transfer coefficients as determined from the Tafel slopes. Also, the observed exponents closely match the theoretical values for mechanism 1 (Table III), supplying further evidence for the validity of this mechanism.

Electrode materials

Tafel plots for various redox couples at a glassy carbon RDE are shown in Fig.4(b). The experimental conditions were identical to those for the measurements at a platinum electrode as shown in Fig.4(a). The estimated transfer coefficients, stoichiometric coefficients, and standard rate constants are summarized in Table VIII. Comparison with the behavior observed at platinum electrodes, allows several conclusions: (1) for the redox couples TETD/$DEDC^-$ and TMTD/$DMDC^-$, the equilibrium potentials established at a glassy carbon electrode (E_{eq}) were shifted in the positive direction with respect to

those at a platinum electrode, indicating that stronger adsorption of the thiolate anions occurs on graphite than on platinum; (2) for FPDS/FPT$^-$ and PDS/PT$^-$, however, the equilibrium potentials were shifted in the negative direction, indicating that stronger adsorption of these organodisulfides takes place on glassy carbon than on platinum; (3) the exchange current densities at glassy carbon electrodes are higher than those at platinum electrodes, and are modified somewhat by the R group in the RSSR molecule.

Tafel plots for TETD/DEDC$^-$ at platinum, graphite, and glassy carbon electrodes are compared in Fig.6(a). An immediate observation is that the exchange current densities or rate constants at graphite electrodes are about an order of magnitude higher than that at platinum electrodes. This is in agreement with a previous cyclic voltammetry study[6], where the separations of peak potentials at graphite electrodes were much smaller than at platinum electrodes. Also, the *apparent* exchange current densities at graphite electrodes are much higher than those at glassy carbon electrodes. This is probably because the surface of the graphite electrode was much rougher or more porous than that of the glassy carbon electrode. Further, the shift of the equilibrium potential from -0.260 V at a platinum electrode to -0.187 V at a glassy carbon electrode can be explained by stronger adsorption of thiolate anions at graphite or glassy carbon relative to platinum[6]. In addition, the measured transfer coefficients at platinum electrodes were slightly more symmetric than those at glassy carbon electrodes.

Tafel polarization of platinum, graphite, and stainless steel electrodes in concentrated RSSR/RS$^-$ solutions at 373 K are shown in Fig.6(b). The cell currents were measured at stationary electrodes while the electrolyte solution was vigorously stirred by a magnetic spin bar. The potential range over which

Tafel polarization was observed was narrow, and deviations at high overpotentials were probably brought about by insufficient mass transport. Nevertheless, in conjunction with the determination of exchange current densities from the slopes of the corresponding linear polarization plots (i vs. η when $|\eta| << RT/F$), the Tafel slopes were determined without ambiguity. The estimated transfer coefficients and the standard rate constants for different electrode materials, averaged over values obtained at different concentrations of TETD and NaDEDC, are summarized in Table IX.

In addition to inert electrodes such as platinum and carbon, stainless steel, aluminum, and copper electrodes were also investigated. Stainless steel electrodes were found to passivate quickly in the electrolyte solution and subsequently behave like platinum electrodes, but the measured exchange current densities were much lower.

Upon immersion of an aluminum electrode in an electrolyte solution containing 1.34 M TETD and 1.34 M NaDEDC in DMSO at 373 K, an initial corrosion potential of -1.6 V was observed, which decayed to approximately -0.36 V in about 30 minutes, and then remained relatively stable. The exchange current at a passivated aluminum electrode was about an order of magnitude lower than that at a passivated stainless steel electrode. Unlike aluminum which passivated slowly, copper electrodes were actively corroded in the electrolyte solution. As soon as a copper electrode was immersed in the electrolyte solution, the portion of the solution adjacent to the electrode surface turned jet black (the color of the copper complex CuDEDC) and the corrosion potential shifted continuously in the positive direction as more copper was corroded.

Electrocatalysis

The behavior of a Na/β"-alumina/RSSR cell with a dimethyldisulfide (DMDS) positive electrode, with and without cobalt phthalocyanine (CoPc) as an electrocatalyst, is shown in Fig.7. The dramatic results demonstrate that the discharge current density for the Na/RSSR cell with CoPc was greatly enhanced relative to the cell without CoPc. In fact, the reduction of Na/RSSR cell overpotential by phthalocyanine addition was observed on both charge and discharge, indicating that electrocatalysis is probably due to adsorbed phthalocyanine on the graphite felt current collector. Other transition metal phthalocyanines and transition metal thio salts, including Co, Fe, Cu, Zn, Ti, etc., were also found to have some catalytic effect. The electrocatalysis of RSSR/RS^- redox couples by adsorbed transition metal phthalocyanines has been reported previously for the related cystine/cysteine redox couple[22]. The use of adsorbed phthalocyanines to enhance the activity of the graphite electrode is analogous the use of *modified electrodes* for similar purposes[23,24]. However, further studies are needed to elucidate the detailed catalytic mechanism.

Conclusions

The observed reaction orders for the RSSR/RS^- redox couples are 1 in the anodic direction and 1/2 in the cathodic direction. The determined transfer coefficients are β and $(1-\beta)$ for the cathodic and anodic process, respectively; this indicates that the rate-determining step is repeated twice ($\nu = 2$) for the completion of the overall reaction. The reaction pathway, therefore, takes the *EC* route (Table I) with the first step, charge transfer,

as the rate-determining step. The kinetics of the electrode reaction, then, are fully described by Eqn.6 to 11.

The transfer coefficients and the standard rate constants for various redox couples at different electrode materials as well as at different temperatures are summarized in Tables V to IX.

Electrocatalysts, such as transition metal phthalocyanines and transition metal thiolate salts have been successfully utilized to assist charge transfer.

The stability of stainless steel and aluminum metals towards the $RSSR/RS^-$ electrolyte solutions makes them likely candidates for Na/RSSR battery-case materials.

Acknowledgement

This work was supported by the Assistant Secretary for Conservation and Renewable Energy, Office of Energy Storage and Distribution, Energy Storage Division of the U.S. Department of Energy under Contract No. DE-AC03-76SF00098 with the Lawrence Berkeley Laboratory.

Abbreviations

$DEDC^-$	diethyl dithiocarbamate anion, $[(C_2H_5)_2NCSS]^-$
$DMDC^-$	dimethyl dithiocarbamate anion, $[(CH_3)_2NCSS]^-$
DMSO	dimethylsulfoxide
FPDS	di-fluorophenyl disulfide, $(F\text{-}C_6H_4\text{-}S\text{-})_2$
FPT^-	fluorophenyl thiolate anion, $[F\text{-}C_6H_4\text{-}S]^-$
DMDS	dimethyldisulfide, $[CH_3\text{-}S\text{-}]_2$
NaDEDC	sodium diethyl dithiocarbamate, $(C_2H_5)_2NCSS\text{-}Na$
NaDMDC	sodium dimethyl dithiocarbamate, $(CH_3)_2NCSS\text{-}Na$
NaFPT	sodium fluorophenyl thiolate, $F\text{-}C_6H_4\text{-}S\text{-}Na$
NaPT	sodium phenyl thiolate, $C_6H_5\text{-}S\text{-}Na$
MPc	metal phthalocyanine
PDS	phenyl disulfide, $(C_6H_5\text{-}S\text{-})_2$
PT^-	phenyl thiolate anion, $[C_6H_5\text{-}S]^-$
R	an organic moiety
RDE	rotating disk electrode
rds	rate-determining step
rpm	revolution per minute
RS^-	a group of thiolate anions
RSSR	a group of organic disulfides
TEAP	tetraethylammonium perchlorate, $(C_2H_5)_4NClO_4$
TETD	tetraethylthiuram disulfide, $((C_2H_5)_2NCSS\text{-})_2$
TMAC	tetramethylammonium chloride, $(CH_3)_4NCl$
TMTD	tetramethylthiuram disulfide, $((CH_3)_2NCSS\text{-})_2$

Notation

A	*electrode area, [cm^2]*
C^*_i	*concentration of species i (i = RS^- or RSSR), [$\mu mol\ cm^{-3}$]*
$C^*_{i,s}$	*concentration of species i at electrode surface, [$\mu mol\ cm^{-3}$]*
$C^*_{i,b}$	*concentration of species i in the bulk solution, [$\mu mol\ cm^{-3}$]*
D_i	*diffusion coefficient of species i, [$cm^2\ sec^{-1}$]*
E	*potential of an electrode versus a reference, [V]*
E_{eq}	*equilibrium potential of an electrode versus a reference, [V]*
F	*Faraday's constant, 96,487[C equiv.$^{-1}$]*
i	*current, [μA]*
i_k	*pure kinetic current as defined by Eqn.5, [μA]*
$i_{k,a}, i_{k,c}$	*pure kinetic current in anodic and direction, [μA]*
i_l	*limiting current, [μA]*
$i_{l,a}, i_{l,c}$	*limiting current in anodic and cathodic direction, [μA]*
i_o	*exchange current, [μA]*
k^o	*standard rate constant, [$(mol/s\text{-}cm^2)(cm^3/mol)^{(\lambda+\mu)}$]*
k_{ai}, k_{ci}	*rate constants in anodic and cathodic direction for elementary step i (i=1,2,3)*
k_f, k_b	*rate constants in forward and backward direction for a chemical reaction*
n	*number of electrons transferred in the overall reaction ($n = \vec{\gamma} + r\nu + \overleftarrow{\gamma}$)*
r	*number of electrons transferred in the rds*
r_i	*reaction rate for elementary step i (i=1,2,3), [mol $cm^{-2}\ s^{-1}$]*
R	*universal gas constant, 8.3143 [J $mol^{-1}\ K^{-1}$]*
T	*absolute temperature, [K]*
α_a, α_c	*transfer coefficients (as defined in Eqn.2 or 5)*
β	*symmetry factor of the rds*
$\beta_{\vec{i}}$	*symmetry factor of elementary step i (i = 1,2,3)*
$\gamma, \overleftarrow{\gamma}$	*number of electrons transferred in the steps preceding and after the rds*
γ_i	*reaction order for species i (i = RS^- or RSSR)*
η	*overpotential at an electrode surface, $\eta = E - E_{eq}$, [V]*
λ, μ	*exponents in concentration dependence of exchange current (see Eqn.4)*
ν	*kinematic viscosity of an electrolyte solution, [$cm^2\ sec^{-1}$]. or stoichiometric coefficient of the rate-determining step*
ω	*rotation speed of disk working electrode, [Hz]*

References

[1] K. M. Abraham, R. D. Rauh, and S. B. Brummer, *Electrochem. Acta.*, **23**, 501 (1978).

[2] K. M. Abraham, L. Pitts, and R. Schiff, *J. Electrochem. Soc.*, **127**, 2545 (1980).

[3] G. Mamantov et al., *J. Electrochem. Soc.*, **127**, 2319 (1980).

[4] R. J. Bones, J. Coetzer, R. C. Gallowway and D. A. Teagle, *J. Electrochem. Soc.*, **134**, 2379 (1987).

[5] S. J. Visco, C. C. Mailhe, L. C. De Jonghe, and M. B. Armand, *J. Electrochem. Soc*. **136**, 661 (1989).

[6] Meilin Liu, S. J. Visco, and L. C. De Jonghe, "Electrochemical properties of organodisulfide/thiolate redox couples", *J. Electrochem. Soc.*, accepted for publication.

[7] Meilin Liu, S. J. Visco, and L. C. De Jonghe, "Electrochemical Investigations of Organodisulfides", Extended Abstract #75, *The Electrochemical Society 174th Annual Meeting*, Chicargo, October 1988.

[8] S. Sarangapani and Ernest Yeager, in "Comprehensive Treatise of Electrochemistry," Volume 9, Prenum, New York, 1 (1981).

[9] M. Enyo, in "Comprehensive Treatise of Electrochemistry," Volume 7, Prenum, New York (1981).

[10] Meilin Liu, S. J. Visco, and L. C. De Jonghe, "Impedance Spectroscopy Studies of Organodisulfides", *J Electrochem. Soc.*, to be submitted.

[11] V. Y. Filinovsky, and Y. V. Pleskov, in "Comprehensive Treatise of Electrochemistry," Volume 9, Prenum, New York, 293 (1981).

[12] F. Opekar and P. Beran, *J. Electroanal. Chem.*, **69**, 1 (1976).

[13] D. Jahn and W. Vielstich, *J Electrochemical Soc.*, **109**, 849 (1962).

[14] A. J. Bard, and L. R. Faulkner, "Electrochemical Methods, Fundamentals and Applications", Wiley, New York, 1980.

[15] J. S. Newman, "Electrochemical Systems", Prentice-Hall, Englewood Cliffs, N.J., 1972.

[16] J. O'M. Bockris and A. K. N. Reddy, "Modern Electrochemistry", Plenum Press, New York, Vol.2 (1970).

[17] P. T. Kissinger, C. R. Preddy, R. E. Shoup and W. R. Heineman, in "Laboratory Techniques in Electroanalytical Chemistry", Marcell Dekker, New York, 9 (1984).

[18] M. W. M. Graef, *J. Electrochem. Soc.*, **132**, 1038(1985).

[19] M. Sakai, J. Osteryoung and R. A. Osteryoung, *J Electrochem. Soc.*, **135**, 3001 (1988).

[20] R. W. Zurilla, R. K. Sen, and E. Yeager, *J. Electrochem. Soc.*, **125**, 1103 (1978).

[21] V. Veskovic, N. Anastasijevie, and R. R. Adzic, *J. Electroanal. Chem.*, **218**, 53 (1987).

[22] J. H. Zagal and P. Herrera, *Electrochem. Acta*, **30**, 449 (1985).

[23] D. E. Bergbreiter, in "Chemically Modified Surfaces in Catalysis and Electrocatalysis", ed. by J. S. Miller, Washington, D. C., American Chemical Society, 1 (1982).

[24] R. W. Murray, *Phil. Trans. R. Soc.*, **A302**, 253 (1981).

Figure Captions

Fig.1 (a) Linear sweep voltammograms for oxidation of FPT^- to FPDS at a platinum disk electrode immersed in electrolyte solution of 2.2 mM NaFPT in DMSO containing 0.1 M TEAP (293 K). The potential sweep rate was 5 mV/s. The numbers adjacent to each curve correspond to rotation speeds in rpm.

(b) Levich plots for oxidation of various thiolate anions to the corresponding disulfide at a platinum electrode. The bulk concentration of thiolate salt in the electrolyte solution was (■) 2.8 mM NaDEDC, (+) 2.4 mM NaDMDC, (△) 2.2 mM NaFPT, and (◇) 2.1 mM NaPT.

Fig.2 (a) The plot of $Log(i_a)$ vs. $Log(1 - i_a/i_{l,a})$ at different rotation speeds for oxidation of thiolate anion FPT^- to disulfide FPDS at a platinum disk electrode at constant potentials. The slopes of the linear plots, γ, represent the anodic reaction order for species FPT^-. Electrolyte solution contained 2.2 mM NaFPT.

(b) The plot of $Log(i_c)$ vs. $Log(1 - i_c/i_{l,c})$ at different rotation speeds for reduction of disulfide FPDS to thiolate anion FPT^- at a platinum disk electrode at constant potentials. The slopes of the linear plots, γ, represent the cathodic reaction orders for species FPDS. Electrolyte solution contained 2.0 mM FPDS.

Fig.3 (a) The reciprocal Levich plot for oxidation of thiolate anion FPT^- to the corresponding disulfide FPDS at a platinum electrode. Electrolyte solution contained 2.2 mM NaFPT.

(b) Tafel plots for oxidation of various thiolate anions to the corresponding disulfides at a platinum electrode (293 K). The kinetic currents, i_k, were determined from the intercept at i^{-1} axis from the reciprical Levich plots similar to Fig.3(a). The bulk concentration of thiolate salt in the electrolyte solution was (■) 2.8 mM NaDEDC, (+) 2.4 mM NaDMDC, and (△) 2.2 mM NaFPT.

Fig.4 Tafel plots for various $RSSR/RS^-$ redox couples at (a) a platinum disk electrode and (b) a glassy carbon electrode. The working electrodes

were rotated at 3000 rpm. The potential sweep rate was 1 mV/s. The electrolyte solution contained bulk concentrations of (■) 2.1 mM TETD and 2.2 mM NaDEDC, (+) 2.6 mM TMTD and 2.4 mM NaDMDC, (△) 2.0 mM FPDS and 2.2 mM NaFPT, and (◊) 1.8 mM PDS and 2.1 mM NaPT.

Fig.5 (a) Dependence of exchange currents on concentration of thiolate anions at constant concentration of the corresponding organodisulfide: (■) 4.0 mM TETD, (+) 4.0 mM TMTD, (△) 4.0 mM FPDS, and (◊) 4.0 mM PDS.

(b) Dependence of exchange currents on concentration of organodisulfides at a constant concentration of the corresponding thiolate salt: (■) 4.0 mM NaDEDC, (+) 4.0 mM NaDMDC, (△) 4.0 mM NaFPT, and (◊) 4.0 mM NaPT.

Fig.6 (a) Tafel plots for the TETD/$DEDC^-$ redox couple at 293 K. The platinum and glassy carbon electrodes were rotated at 3000 rpm. The graphite electrode was held stationary while the electrolyte solution was vigourously stirred during measurements. Electrolyte solution included 2.0 mM TETD and 2.0 mM MaDEDC.

(b) Tafel plots for the TETD/$DEDC^-$ redox couple at 373 K. Cell currents were monitered across stationary electrodes of platinum, graphite, and stainless steel while the electrolyte solution was stirred vigourously and purged with dry argon. Electrolyte solutions included 1.34 M TETD and 1.34 M MaDEDC. The established equilibrium potentials were -0.349 V at platinum (■), -0.313 V at graphite (△), and -0.348 V at stainless steel (◊).

Fig.7 Discharge curves for a Na/β"-alumina/RSSR cell (initial capacity: 2000 coulombs) having a dimethyldisulfide (DMDS) cathode: (+) without electrocatalyst, (■) with cobalt phathalocyanine (5 coulombs) electrocatalyst. Cell operating temperature was 378 K.

Table I

Possible reaction pathways and the corresponding mechanisms for oxidation of thiolate anions to organodisulfides			
reaction route		rds	mechanism #
(1) EC route	$2\left\{RS^- \underset{k_{c1}}{\overset{k_{e1}}{\rightleftharpoons}} RS\cdot + e^-\right\}$ (1-1)	1st	1
	$2\,RS\cdot \underset{k_b}{\overset{k_f}{\rightleftharpoons}} RSSR$ (1-2)	2nd	2
(2) ECE route	$RS^- \underset{k_{c1}}{\overset{k_{e1}}{\rightleftharpoons}} RS\cdot + e^-$ (2-1)	1st	3
	$RS^- + RS\cdot \underset{k_b}{\overset{k_f}{\rightleftharpoons}} RSSR^-$ (2-2)	2nd	4
	$RSSR^- \underset{k_{c3}}{\overset{k_{e3}}{\rightleftharpoons}} RSSR + e^-$ (2-3)	3rd	5
(3) CEE route	$2\,RS^- \underset{k_b}{\overset{k_f}{\rightleftharpoons}} {}^-RSSR^-$ (3-1)	1st	6
	${}^-RSSR^- \underset{k_{c2}}{\overset{k_{e2}}{\rightleftharpoons}} RSSR^- + e^-$ (3-2)	2nd	7
	$RSSR^- \underset{k_{c3}}{\overset{k_{e3}}{\rightleftharpoons}} RSSR + e^-$ (3-3)	3rd	identical to #5
(4) EEC route	$RS^- \underset{k_{c1}}{\overset{k_{e1}}{\rightleftharpoons}} RS\cdot + e^-$ (4-1)	1st	identical to #3
	$RS\cdot \underset{k_{c2}}{\overset{k_{e2}}{\rightleftharpoons}} RS^+ + e^-$ (4-2)	2nd	8
	$RS^+ + RS^- \underset{k_b}{\overset{k_f}{\rightleftharpoons}} RSSR$ (4-3)	3rd	9

Table II

Kinetic equations and the corresponding reaction orders, transfer coefficients, and stoichiometric coefficients for 9 possible reaction mechanisms listed in Table I						
mechanism #	overall reaction rate ($mol\ cm^{-2}\ sec^{-1}$)	reaction order		transfer coef.		stoic. coef.
		γ_{RS-}	γ_{RSSR}	α_a	α_c	ν
1	$r_1 = k_{a1}(C_{RS-})\exp[\frac{(1-\beta_1)FE}{RT}] - k_{c1}(\frac{k_b}{k_f})^{\frac{1}{2}}(C_{RSSR})^{\frac{1}{2}}exp[-\frac{\beta_1 FE}{RT}]$	1	$\frac{1}{2}$	$1-\beta_1$	β_1	2
2	$r_2 = k_f\frac{k_{a1}}{k_{c1}^2}(C_{RS-})^2\exp[\frac{2FE}{RT}] - k_b C_{RSSR}$	2	1	2	0	1
3	$r_1 = k_{a1}(C_{RS-})\exp[\frac{(1-\beta_1)FE}{RT}] - k_{c1}\frac{k_b k_{c3}}{k_f k_{a3}}(\frac{C_{RSSR}}{C_{RS-}})exp[-\frac{(1+\beta_1)FE}{RT}]$	1	1	$1-\beta_1$	$1+\beta_1$	1
4	$r_2 = k_f\frac{k_{a1}}{k_{c1}}(C_{RS-})^2\exp[\frac{FE}{RT}] - k_b\frac{k_{c3}}{k_{a3}}(C_{RSSR})exp[-\frac{FE}{RT}]$	2	1	1	1	1
5	$r_3 = k_{a3}\frac{k_f k_{a1}}{k_b k_{c1}}(C_{RS-})^2\exp[\frac{(2-\beta_3)FE}{RT}] - k_{c3}(C_{RSSR})exp[-\frac{\beta_3 FE}{RT}]$	2	1	$2-\beta_3$	β_3	1
6	$r_1 = k_f(C_{RS-})^2 - k_b\frac{k_{c2}k_{c3}}{k_{a2}k_{a3}}(C_{RSSR})exp[-\frac{2FE}{RT}]$	2	1	0	2	1
7	$r_2 = k_{a2}\frac{k_f}{k_b}(C_{RS-})^2\exp[\frac{(1-\beta_2)FE}{RT}] - k_{c2}\frac{k_{c3}}{k_{a3}}(C_{RSSR})exp[-\frac{(1+\beta_2)FE}{RT}]$	2	1	$1-\beta_2$	$1+\beta_2$	1
8	$i_2 = k_{a2}\frac{k_{a1}}{k_{c1}}C_{RS-}\exp[\frac{(2-\beta_2)FE}{RT}] - k_{c2}\frac{k_b}{k_f}\frac{C_{RSSR}}{C_{RS-}}\exp[-\frac{\beta_2 FE}{RT}]$	1	1	$2-\beta_2$	β_2	1
9	$r_3 = k_f\frac{k_{a1}k_{a2}}{k_{c1}k_{c2}}C_{RS-}^2\exp[\frac{2FE}{RT}] - k_b C_{RSSR}$	2	1	2	0	1

* $\gamma_{RS-} = (\frac{\partial \ln(i_a)}{\partial \ln(C_{RS-})})_{C_{RSSR},E}$

** $\gamma_{RSSR} = (\frac{\partial \ln(i_c)}{\partial \ln(C_{RSSR})})_{C_{RS-},E}$

Table III

Dependence of exchange currents on concentrations of organodisulfide/thiolate salt for the possible reaction mechanisms listed in Table I			
mechanism #	**exchange current**	μ^{*}	λ^{**}
1	$i_o = AFk^o(C_{RS-})^{\beta_1}(C_{RSSR})^{\frac{(1-\beta_1)}{2}}$	β_1	$\frac{(1-\beta_1)}{2}$
2	$i_o = 2AFk^o C_{RSSR}$	**0**	**1**
3	$i_o = 2AFk^o(C_{RS-})^{\beta_1}(C_{RSSR})^{\frac{(1-\beta_1)}{2}}$	β_1	$\frac{(1-\beta_1)}{2}$
4	$i_o = 2AFk^o C_{RS-}(C_{RSSR})^{1/2}$	**1**	**½**
5	$i_o = 2AFk^o(C_{RS-})^{\beta_3}(C_{RSSR})^{1-\frac{\beta_3}{2}}$	β_3	$(1-\frac{\beta_3}{2})$
6	$i_o = 2AFk^o(C_{RS-})^2$	**2**	**0**
7	$i_o = 2AFk^o(C_{RS-})^{(1+\beta_2)}(C_{RSSR})^{\frac{(1-\beta_2)}{2}}$	$(1+\beta_2)$	$\frac{(1-\beta_2)}{2}$
8	$i = 2AFk^o(C_{RS-})^{(\beta_2-1)}(C_{RSSR})^{(1-\frac{\beta_2}{2})}$	(β_2-1)	$(1-\frac{\beta_2}{2})$
9	$i = 2AFk^o C_{RSSR}$	**0**	**1**

* $\mu = (\frac{\partial \ln(i_o)}{\partial \ln(C_{RS-})})_{C_{RSSR}}$

** $\lambda = (\frac{\partial ln(i_o)}{\partial \ln(C_{RSSR})})_{C_{RS-}}$

Table IV

Calculated diffusion coefficients of thiolate anions (from RDE measurements at 293 K)			
thiolate anion	C_{RS^-} $\mu mol\ cm^{-3}$	viscosity $cm^2\ s^{-1}$	diffusion coefficient $10^6 cm^2\ s^{-1}$
$DEDC^-$	2.8	0.02178	3.13 ± 0.28
$DMDC^-$	2.4	0.02165	3.17 ± 0.21
FPT^-	2.2	0.02183	1.48 ± 0.10
PT^-	2.1	0.02214	0.67 ± 0.06

Table V

Observed reaction orders and anodic transfer coefficients for organodisulfide/thiolate redox couples at platinum electrode (determined fron RDE measurements at 293 K)			
$RSSR/RS^-$	reaction order		transfer coefficient
	γ_{RS-}	γ_{RSSR}	α_a
$TETD/DEDC^-$	0.91 ± 0.05	0.49 ± 0.01	0.65 ± 0.017
$TMTD/DMDC^-$	0.87 ± 0.06	0.49 ± 0.03	0.64 ± 0.027
$FPDS/FPT^-$	0.89 ± 0.03	0.51 ± 0.02	0.51 ± 0.019
PDS/PT^-	0.90 ± 0.04	0.53 ± 0.03	-

Table VI

Observed transfer coefficients, stoichiometric coefficients, and standard rate constants for organodisulfide/thiolate redox couples at platinum electrodes (determined from polarization measurements at 293 K)							
$RSSR/RS^-$	concentration $\mu mol\ cm^{-3}$		equilibrium potential	transfer coefficient		stoichiometric coefficient	standard rate constant
	C_{RSSR}	C_{RS-}	$E_{eq}\,(V)$	α_a	α_c	ν	k^o x 10^8
$TETD/DEDC^-$	2.1	2.2	-0.260 ± 0.009	0.66 ± 0.006	0.36 ± 0.005	2 ± 0.021	0.34 ± 0.08
$TMTD/DMDC^-$	2.6	2.4	-0.256 ± 0.012	0.67 ± 0.011	0.34 ± 0.006	2 ± 0.025	1.11 ± 0.14
$FPDS/FPT^-$	2.0	2.2	-0.397 ± 0.014	0.51 ± 0.007	0.52 ± 0.006	2 ± 0.031	0.63 ± 0.12
PDS/PT^-	1.8	2.1	-0.512 ± 0.011	0.42 ± 0.009	0.56 ± 0.011	2 ± 0.034	0.51 ± 0.06

Table VII

Dependence of exchange currents at platinum electrode on concentrations of organodisulfides/thiolate salts (determined from polarization measurements at 293 K)		
$RSSR/RS^-$	exponents	
	λ	μ
$TETD/DEDC^-$	0.33 ± 0.02	0.34 ± 0.03
$TMTD/DMDC^-$	0.32 ± 0.03	0.37 ± 0.04
$FPDS/FPT^-$	0.24 ± 0.03	0.52 ± 0.05
PDS/PT^-	0.23 ± 0.04	0.54 ± 0.03

Table VIII

Observed transfer coefficients, stoichiometric coefficients, and standard rate constants for organodisulfide/thiolate redox couples at glassy carbon electrodes (determined from polarization measurements at 293 K)							
$RSSR/RS^-$	concentration $\mu mol\ cm^{-3}$		equilibrium potential	transfer coefficient		stoichiometric coefficient	standard rate constant
	C_{RSSR}	C_{RS-}	$E_{eq}\,(V)$	α_a	α_c	ν	$k^o \times 10^8$
$TETD/DEDC^-$	2.1	2.2	-0.187 ± 0.013	0.69 ± 0.007	0.31 ± 0.006	2 ± 0.013	0.89 ± 0.13
$TMTD/DMDC^-$	2.6	2.4	-0.133 ± 0.011	0.63 ± 0.013	0.37 ± 0.007	2 ± 0.021	1.8 ± 0.16
$FPDS/FPT^-$	2.0	2.2	-0.441 ± 0.009	0.35 ± 0.011	0.67 ± 0.019	2 ± 0.051	2.3 ± 0.14
PDS/PT^-	1.8	2.1	-0.523 ± 0.012	0.47 ± 0.013	0.59 ± 0.016	2 ± 0.065	1.62 ± 0.12

Table IX

Observed transfer coefficients and standard rate constants for $TETD/DEDC^-$ at different electrode materials				
electrode material	transfer coefficient		standard rate constant	
	α_a	α_c	$k^o \times 10^8\,(293\ K)$	$k^o \times 10^7\,(373\ K)$
platinum	0.65 ± 0.009	0.35 ± 0.008	0.34 ± 0.09	1.25 ± 0.28
glassy carbon	0.67 ± 0.015	0.33 ± 0.013	0.91 ± 0.16	
graphite	0.67 ± 0.021	0.33 ± 0.023	2.96 ± 0.44	9.45 ± 0.86
stainless steel	0.64 ± 0.021	0.36 ± 0.018		0.24 ± 0.056

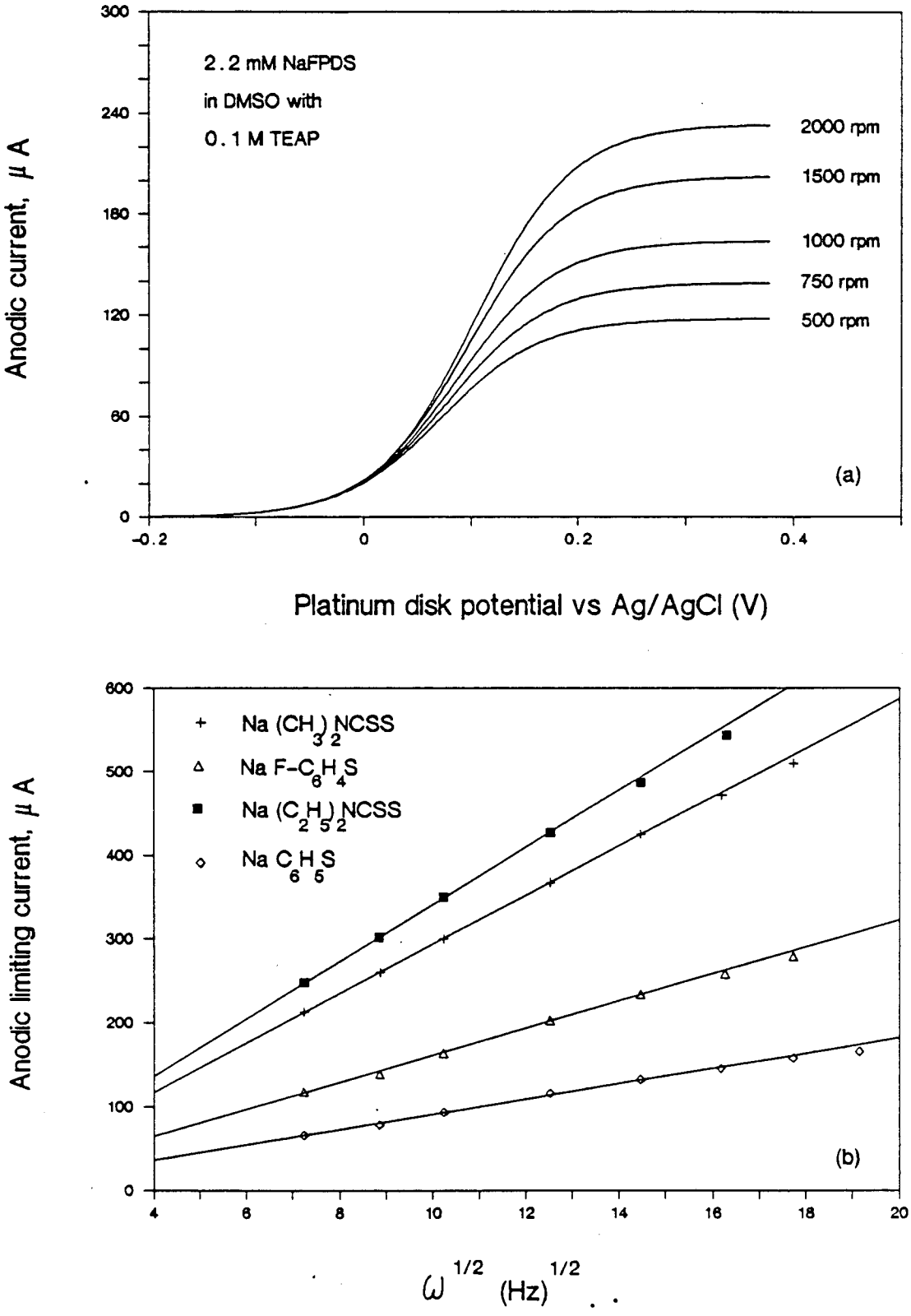
2.2 mM NaFPDS
in DMSO with
0.1 M TEAP
2000 rpm
1500 rpm
1000 rpm
750 rpm
500 rpm
(a)
Anodic current, μA
Platinum disk potential vs Ag/AgCl (V)
Na (CH3)2NCSS
Na F-C6H4S
Na (C2H5)2NCSS
Na C6H5S
(b)
Anodic limiting current, μA
ω^1/2 (Hz)^1/2

Fig. 1

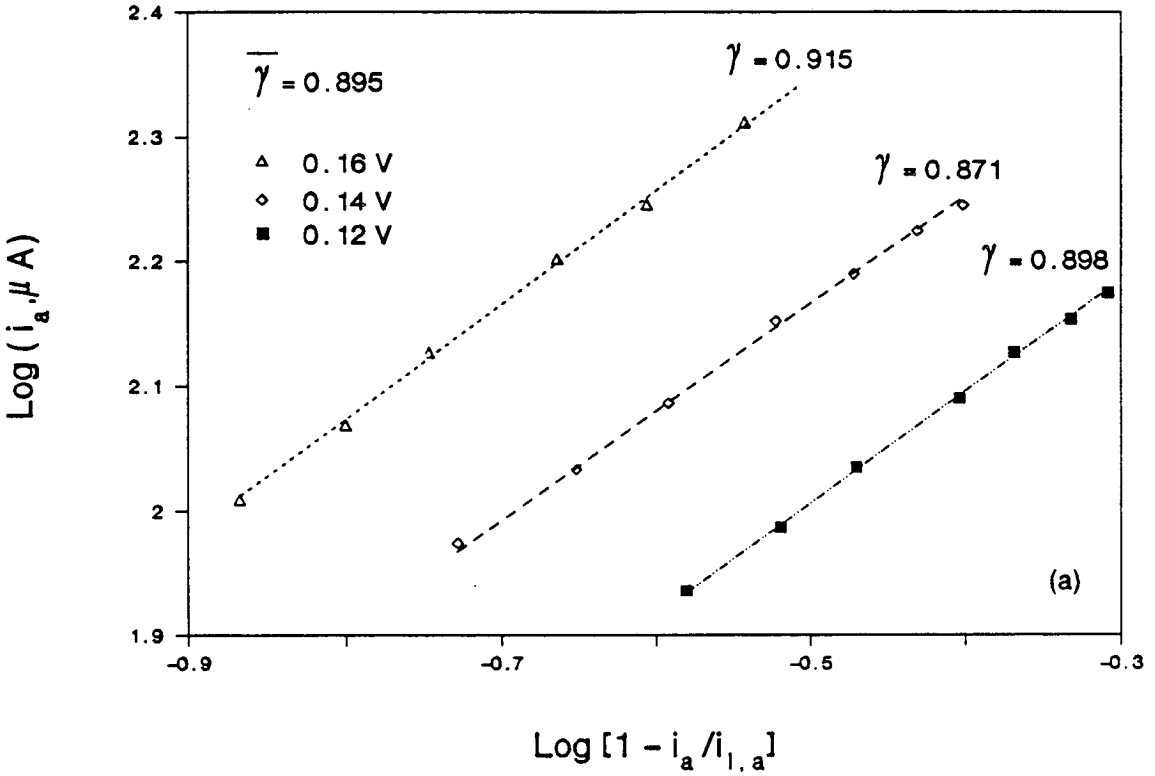
$\overline{\gamma}$ = 0.895
γ = 0.915
γ = 0.871
γ = 0.898
0.16 V
0.14 V
0.12 V
(a)
Log (i_a ,μ A)
Log [1 – i_a /$i_{l,a}$]

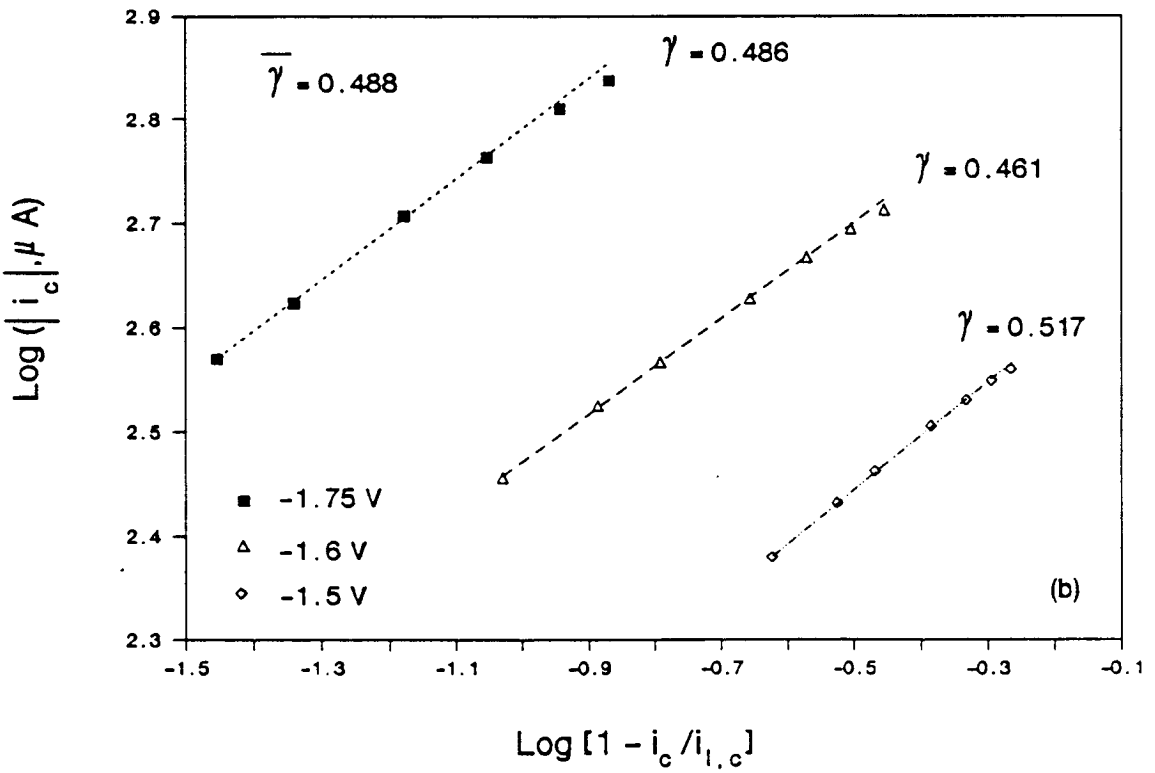
$\overline{\gamma}$ = 0.488
γ = 0.486
γ = 0.461
γ = 0.517
-1.75 V
-1.6 V
-1.5 V
(b)
Log (| i_c |,μ A)
Log [1 – i_c /$i_{l,c}$]

Fig. 2

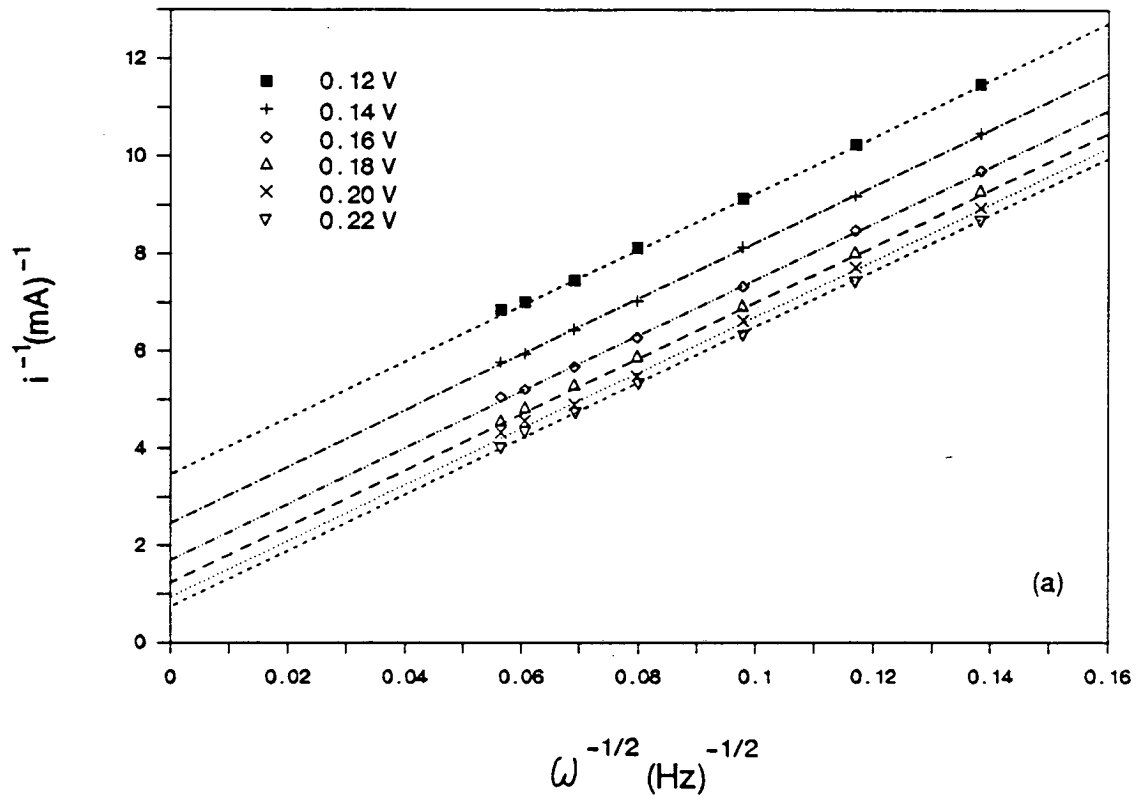
0.12 V
0.14 V
0.16 V
0.18 V
0.20 V
0.22 V
(a)
$i^{-1}(mA)^{-1}$
$\omega^{-1/2}$ $(Hz)^{-1/2}$

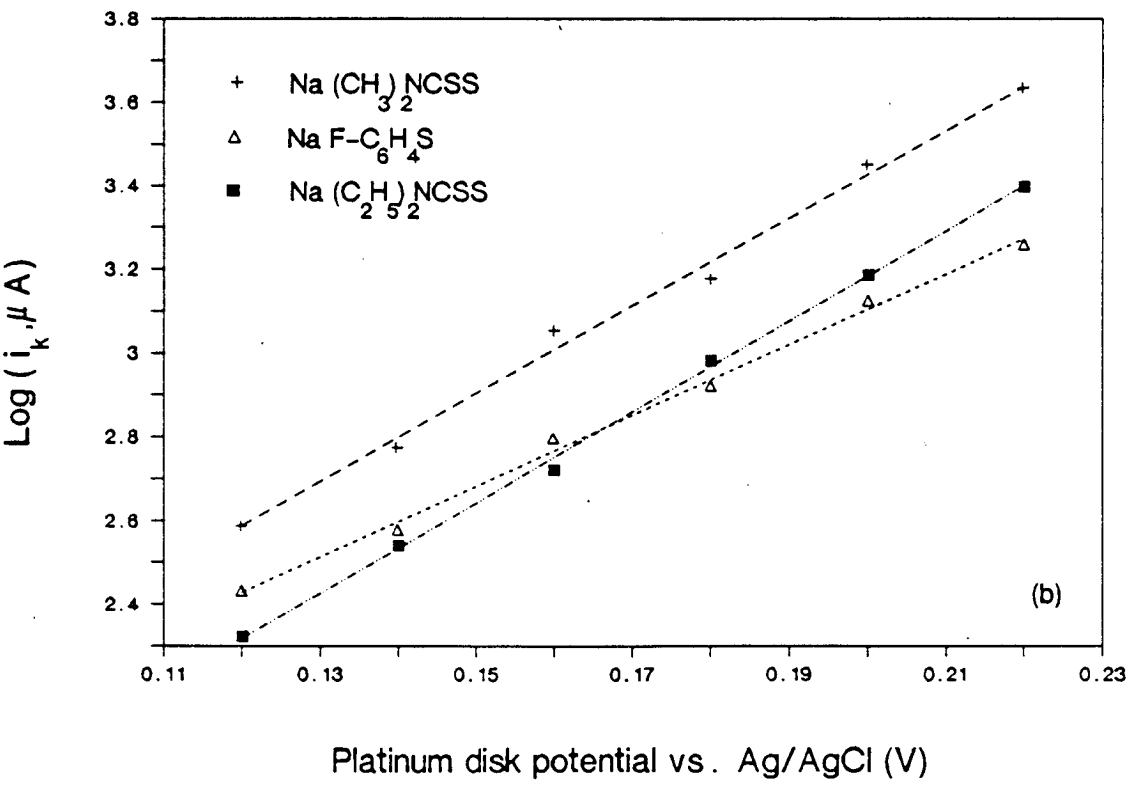
Na $(CH_3)_2NCSS$
Na F-C_6H_4S
Na $(C_2H_5)_2NCSS$
(b)
Log (i_k ,μ A)
Platinum disk potential vs. Ag/AgCl (V)

Fig. 3

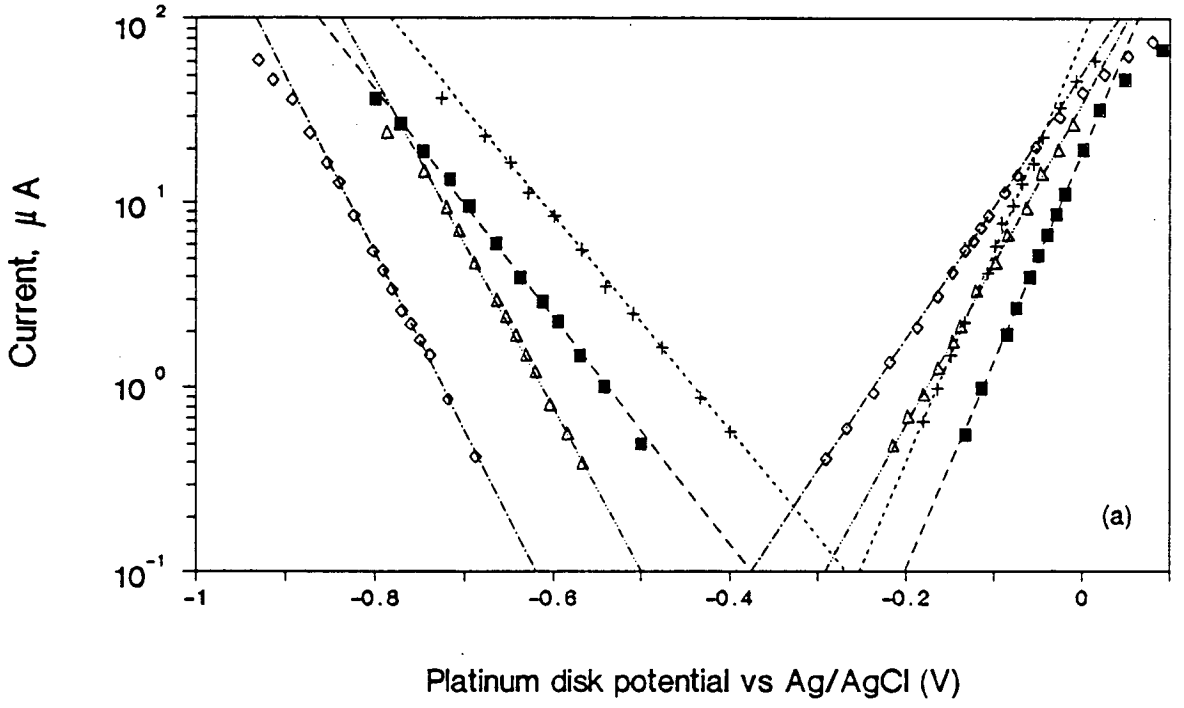
Current, μA
10 2
10 1
10 0
10 -1
-1
-0.8
-0.6
-0.4
-0.2
0
(a)
Platinum disk potential vs Ag/AgCl (V)

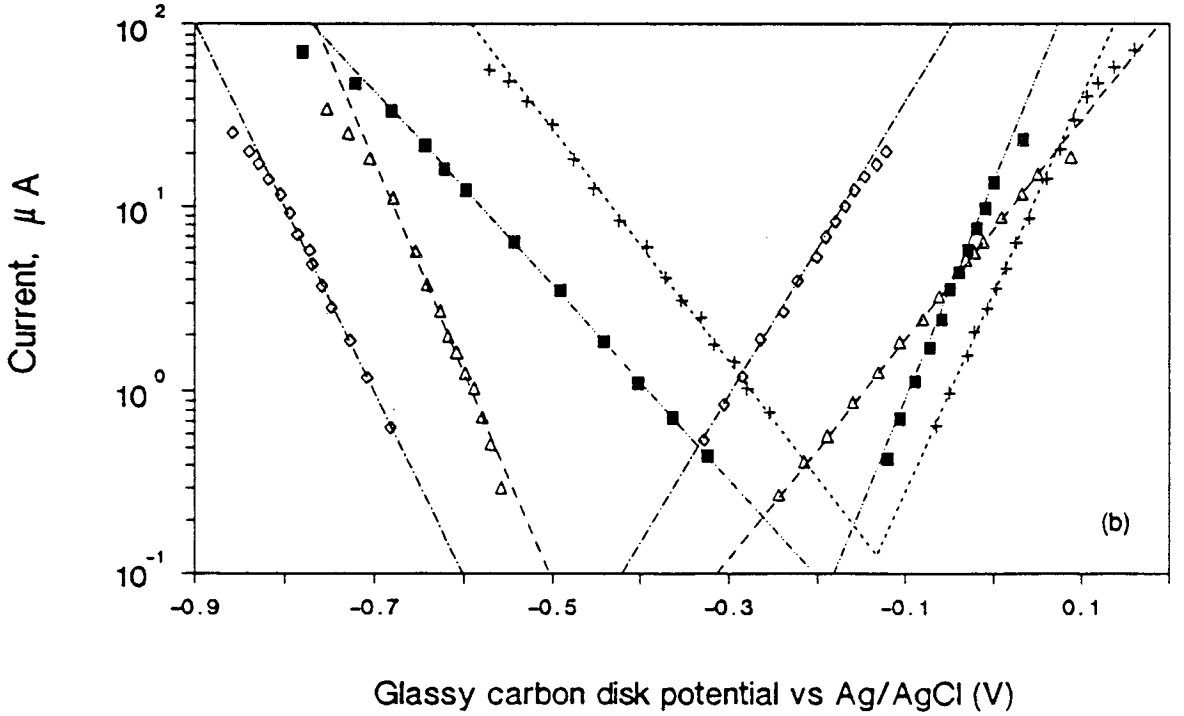
Current, μA
10 2
10 1
10 0
10 -1
-0.9
-0.7
-0.5
-0.3
-0.1
0.1
(b)
Glassy carbon disk potential vs Ag/AgCl (V)

Fig. 4

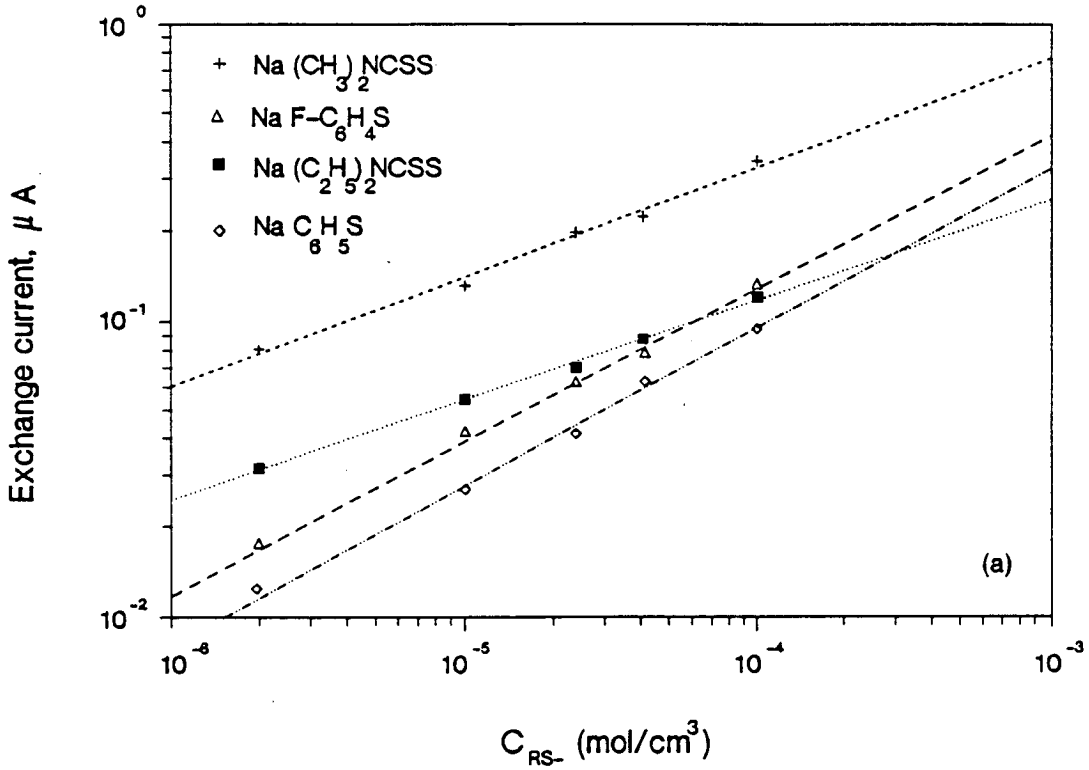
Exchange current, μ A
10 0
10 -1
10 -2
Na (CH3)2NCSS
Na F-C6H4S
Na (C2H5)2NCSS
Na C6H5S
(a)
10 -6
10 -5
10 -4
10 -3
C RS- (mol/cm3)

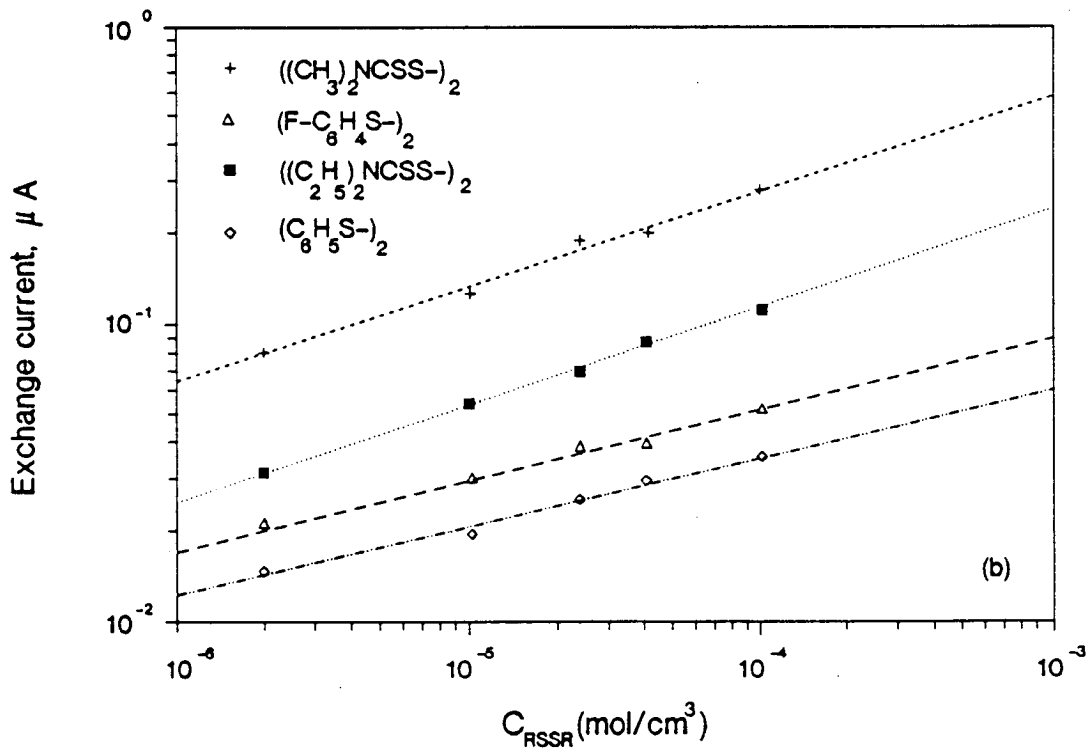
Exchange current, μ A
10 0
10 -1
10 -2
((CH3)2NCSS-)2
(F-C6H4S-)2
((C2H5)2NCSS-)2
(C6H5S-)2
(b)
10 -6
10 -5
10 -4
10 -3
CRSSR(mol/cm3)

Fig. 5

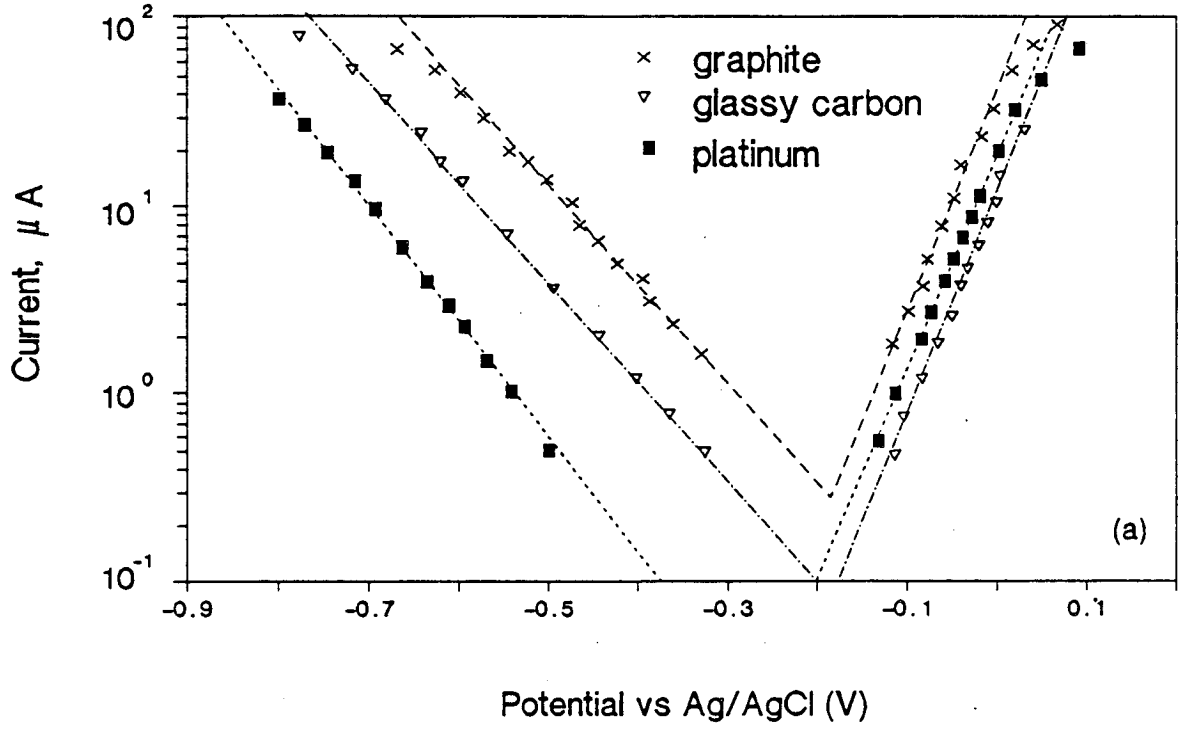
graphite
glassy carbon
platinum
(a)
Current, μ A
Potential vs Ag/AgCl (V)

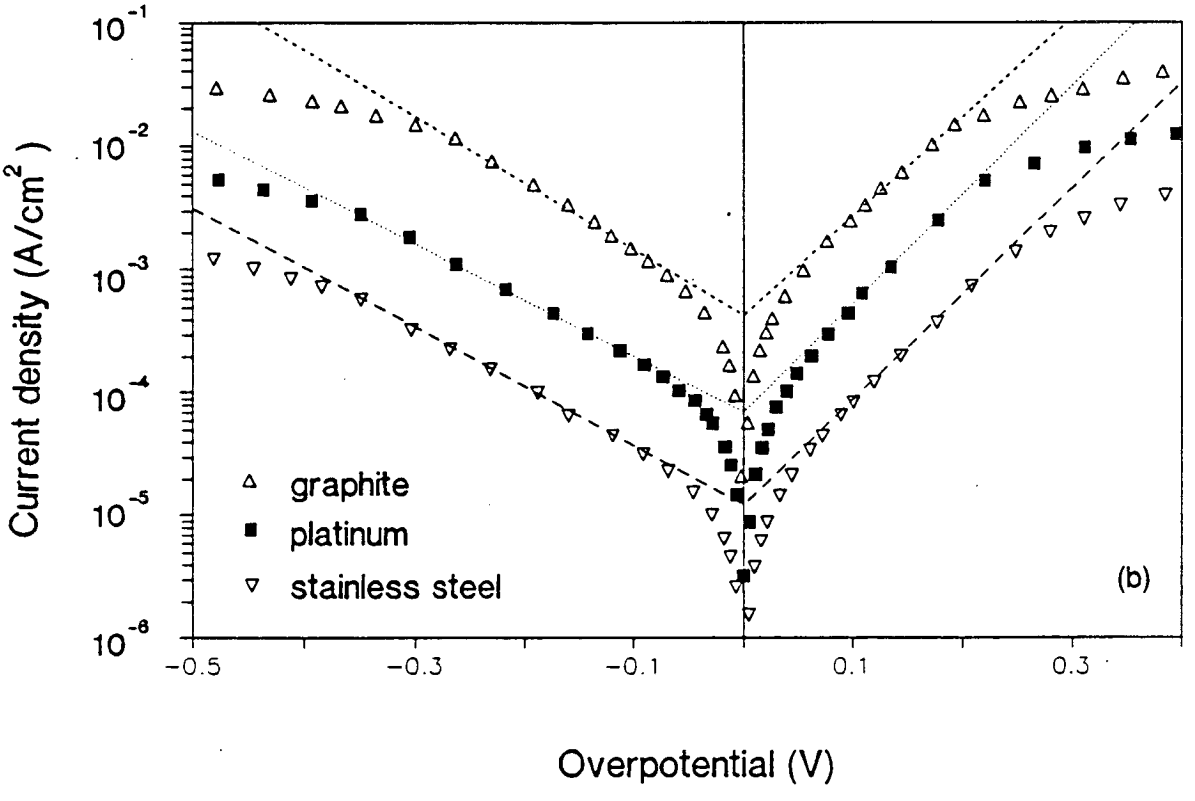
graphite
platinum
stainless steel
(b)
Current density (A/cm²)
Overpotential (V)

Fig. 6

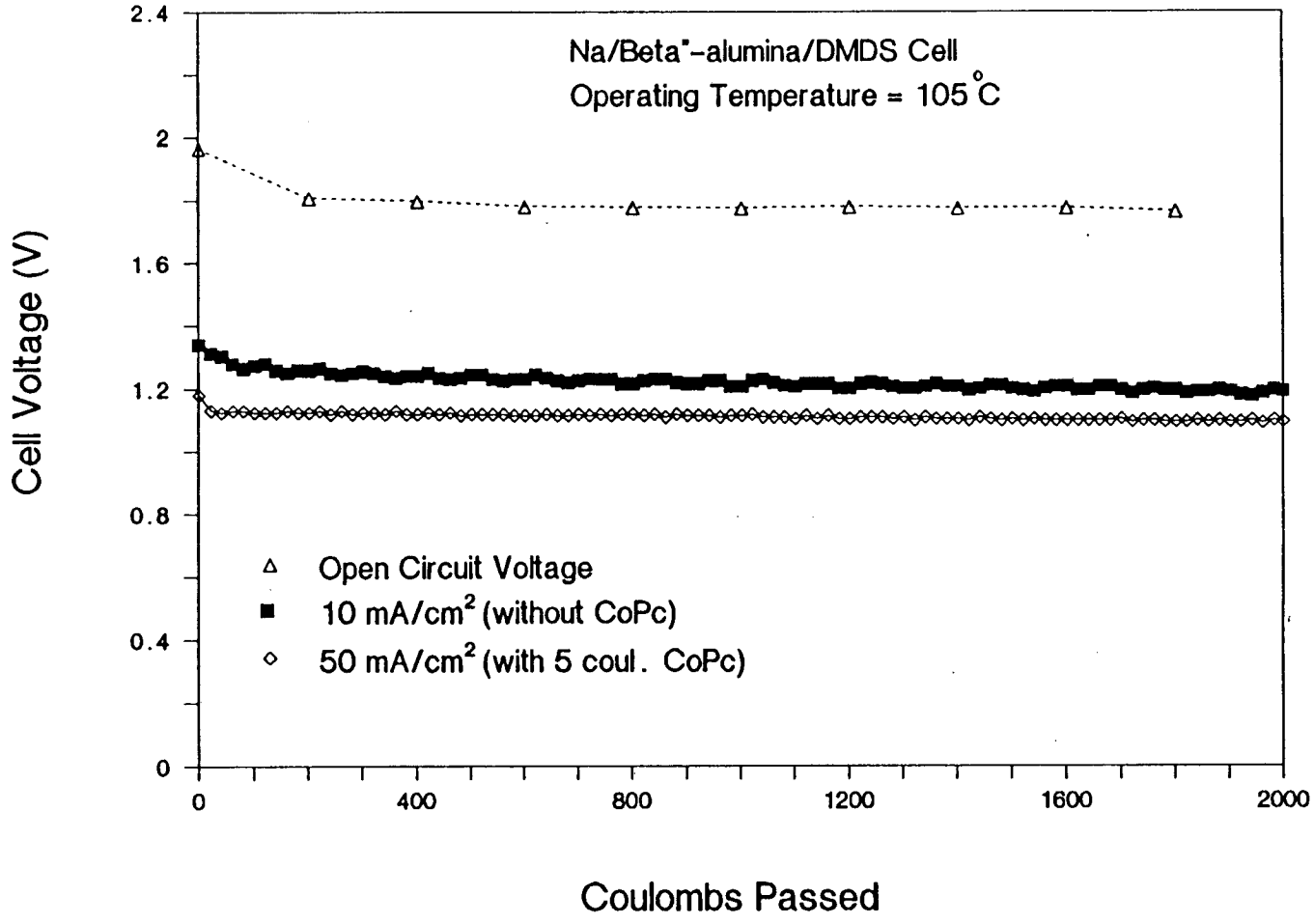
Na/Beta"-alumina/DMDS Cell
Operating Temperature = 105 °C
Cell Voltage (V)
2.4
2
1.6
1.2
0.8
0.4
0
0
400
800
1200
1600
2000
Coulombs Passed
Open Circuit Voltage
10 mA/cm² (without CoPc)
50 mA/cm² (with 5 coul. CoPc)

Fig. 7

LAWRENCE BERKELEY LABORATORY
TECHNICAL INFORMATION DEPARTMENT
1 CYCLOTRON ROAD
BERKELEY, CALIFORNIA 94720